JACS
JOURNAL OF THE AMERICAN CHEMICAL SOCIETY

ARTICLE

pubs.acs.org/JACS

Adsorption of Short-Chain Thiols and Disulfides onto Gold under Defined Mass Transport Conditions: Coverage, Kinetics, and Mechanism

Layal L. Rouhana, Maroun D. Moussallem, and Joseph B. Schlenoff*

Department of Chemistry and Biochemistry, The Florida State University, Tallahassee, Florida 32306, United States

Supporting Information

ABSTRACT: The adsorption of water-soluble alkane thiols and their corresponding disulfides onto gold was followed in real time using highly sensitive surface conductivity measurements. Particular attention was paid to producing clean surfaces and to the purity of the adsorbates. The rate of mass transport to the surface was constant, controlled, and measured, over the whole time course of the experiment ($1-10^4$ s), by convective diffusion. An adsorption rate equation derived for coupled steady state convective-diffusion mass transport and Langmuir kinetics shows that systems limited by mass transport must *also* be slowed by Langmuir kinetics. Thiols and disulfides adsorbed at the same rate, limited mainly by mass transport. The distinct slowdown in adsorption rate for longer alkanethiols, attributed to conformational transitions (lying down → standing up), was less evident for the neutral thiols/disulfides. The slower rate of charged thiol adsorption is thought to stem from steric interactions of large, hydrated tail groups, although calcium as a counterion accelerated monolayer formation. The adsorption kinetics of a charged thiol were almost the same under screened (by extra added salt) or unscreened conditions. Therefore, long-range electrostatic interactions appear to be less important than short-range steric ones in limiting adsorption rates at surfaces.

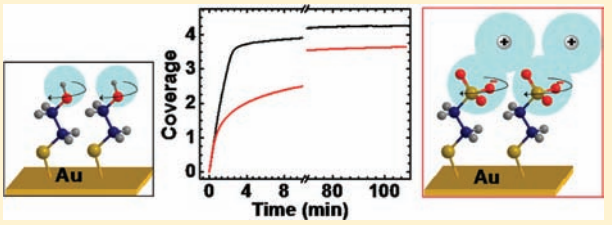

INTRODUCTION

Thiols or disulfides adsorb to gold surfaces to yield thiolate monolayers (self-assembled monolayers, SAMs) according to eqs 1 and 2.[1]

$$2R-SH + 2Au_{(s)} \rightarrow 2RS-Au_{(s)} + H_2 \quad (1)$$

$$RS-SR + 2Au_{(s)} \rightarrow 2RS-Au_{(s)} \quad (2)$$

Following extensive characterization by spectroscopy, diffraction, and microscopy, agreement on the structure of the final, packed monolayer has converged, as summarized in review articles.[2] However, research on the kinetics of assembly has produced widely divergent results. The time it takes to form a "full" monolayer has been reported to vary from seconds[3] to minutes,[4] up to several hours,[5] and sometimes days.[6]

Lack of agreement can be traced to several technical and experimental challenges. First, adsorption kinetics are understood to be intrinsically complex as the rate is thought to be controlled by different factors depending on the coverage. For example, long-chain alkanethiols are believed to adsorb first in a "lying down" configuration, where the alkane chain interacts with the surface. The molecule then adopts a "standing up" mode as more adsorbs, and then at high coverage there is believed to be a long-term reorganization where the tail groups pack into a dense, pseudocrystalline structure.[2f,7] Second, despite the fact that the cleanliness of the gold surface is widely acknowledged to be critical to adsorption kinetics, the existence of a clean, reproducible starting surface is rarely verified. Surface purity is often overlooked or assumed because thiols and disulfides are strongly adsorbing systems and they are believed to eventually displace impurities or contaminants, yielding reproducible monolayers. Third, the accurate measurement of surface excess at low coverages is a technical challenge, especially if time resolution on the order of seconds is required and the measurements are to be done in situ. The quartz crystal microbalance provides the right magnitude of sensitivity and resolution,[3c,5b,8a,−8f] but it does not distinguish between surface excess of adsorbate and solvent. Surface plasmon spectroscopy has also been employed.[9] Radiochemical methods have the appropriate sensitivity but lack the required time resolution.[10] Surface conductance was introduced by Rubini[11] and then used by Bohn and co-workers,[12] and other researchers[13] for exquisitely sensitive in situ measurements of adsorbed thiols. This method relies on the change of conductance of a thin film of gold upon chemisorption of a species to the surface.

We sought, in the present work, to address these challenges in several ways. In order to reduce the complexity of the adsorption process, and the analysis of kinetics, we employed short-chain thiols, where the interaction with the surface should be mainly due to the sulfur moiety with little contribution from tail−surface

Received: May 6, 2011
Published: August 11, 2011

dx.doi.org/10.1021/ja2041833 | J. Am. Chem. Soc. 2011, 133, 16080–16091

or tail−tail packing interactions (i.e., lying down → standing up and crystallization transitions).[14] The use of aqueous systems ensures the extraordinary purity of the solvent (as compared to an organic solvent, where the last few ppm of impurity are hard to remove). As discussed later, the use of micromolar concentrations of thiol or disulfide minimizes the contributions of any added impurities (such as residual thiols in disulfides or vice versa) to the adsorption kinetics. Finally, the surface conductance method provides data of exceptional quality, even for the low coverage regime where any complicating thiol−thiol interactions would be minimized.[12]

In addition to the kinetics and final monolayer coverage, the system and techniques chosen allowed us to evaluate several fundamental questions such as a comparison of the rate of thiol versus disulfide adsorption. While it has been known from the early work of Biebuyck and co-workers[1g,15] that both yield the same eventual monolayer, relative kinetics are less clear. For example, some studies suggest that the assembly occurs at the same rate,[1g,15] and others conclude that disulfides having the same number of thiolate units adsorb more slowly[5a,c,16a−16c] or in some cases faster[17] than the respective thiols. The central question of whether adsorption kinetics are controlled by diffusion to the surface, as deduced by some,[10b,18] but not others,[8a,19a−19h] remains. Such a question can only be answered definitively if the mass transport rate is controlled throughout the experiment. Finally, of broad interest to surface science is the difference in adsorption kinetics and coverage for charged versus neutral molecules.[2c, 20a−20c] In this work, we evaluate each of these questions quantitatively.

EXPERIMENTAL SECTION

All aqueous solutions were prepared using deionized water (Barnstead, E-pure, Milli-Q, 18 MΩ cm). 2-Mercaptoethanol (J.T. Baker) was tested for contamination with the respective disulfide using reverse phase liquid chromatography (see Supporting Information). 2-Mercaptoethanesulfonic acid solution (Fluka) was titrated with ultrahigh purity sodium hydroxide (Sigma-Aldrich), cesium hydroxide (J.T. Baker), and calcium hydroxide (J.T. Baker) to yield thiols with various counterions. Potassium ferricyanide (Sigma Aldrich) was 99.99% pure. Hydroxyethyl disulfide (TCI America) was used as purchased. Au and Cr (Refining Systems Inc.) used for evaporation were 99.99% pure. All reagents were purchased at the highest degree of purity available and were used as received.

Scheme S1 in the Supporting Information shows a diagram of the four point resistivity measurement setup. Resistance measurements were performed using a Au thin film (25 mm × 7.5 mm × 14 nm) evaporated on a Cr (5 nm) primed microscope glass slide. Four "thick" Au electrodes (5 nm Cr; 150 nm Au) with contacts to the thin film were then evaporated on the same glass substrate and served as the four point resistance measurement probe. Current was applied to the two outer electrodes, and the voltage between the two inner ones was recorded, for a geometric surface area of 2 mm × 7.5 mm. The deposition rate for the thin Au film was 1 Å/s at pressures lower than 5×10^{-6} Torr. The thickness of the films was checked by profilometry (Tencor instruments) and atomic force microscopy (AFM; Asylum Research Inc., Santa Barbara, CA). The freshly deposited films were subjected to the following treatment before use in the series of four-point resistivity measurements: 10 min dipping in 1 mM potassium hydroxide, a quick rinse in a concentrated H_2SO_4 solution, and then soaking in 0.2 mM thiol solutions for 24 h. Each step was followed by a thorough rinse with deionized water (18 MΩ cm).

A circuit board was clamped to the glass substrate, where spring loaded Au contacts were pressed against the four electrodes. A 50 mA current (General Resistance Instruments, model E-35) was applied throughout the resistivity measurements, which was in the linear ohmic regime of the thin films. The resulting voltage was recorded using a Keithley 196 multimeter, at a frequency of 2 Hz, and collected over a GPIB card by a routine written in LabView. The thin film was dipped vertically into a thermostatted glass cell maintained at 20 °C. The setup was designed in such a way that the film was held at a constant distance from the cell bottom, for reproducibility purposes between all runs. A well-defined constant stirring rate was established using a glass coated magnetic stir bar. The system was sealed other than a needle opening through which the thiols/disulfides were introduced. For the self-assembly study of neutral molecules, 1-mercaptoethanol (MESH) and its respective disulfide 2,2′-dithiodiethanol (MESH-SS) were used. Hydrogen 2-mercaptoethane sulfonate (MESA) was employed as the negatively charged thiol. It was titrated with the corresponding hydroxides to yield sodium 2-mercaptoethane sulfonate (MESA-Na), cesium 2-mercaptoethane sulfonate (MESA-Cs), and calcium 2-mercaptoethane sulfonate (MESA-Ca) (Scheme 1).

Scheme 1. Structures of the Thiols Used in Self Assembly Studies[a]

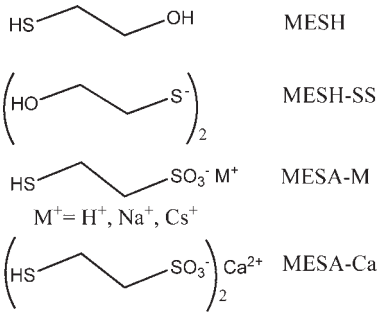

[a] From top to bottom: 1-mercaptoethanol (MESH), 2,2′-dithiodiethanol (MESH-SS), hydrogen 2-mercaptoethane sulfonate (MESA), sodium 2-mercaptoethane sulfonate (MESA-Na), cesium 2-mercaptoethane sulfonate (MESA-Cs), and calcium 2-mercaptoethane sulfonate (MESA-Ca).

A typical run included a background collection in deionized water for 10 min, then the thiol or disulfide was introduced, under a fixed stirring rate, and the resulting signal (in the range of 110−120 mV) was recorded for varied periods of time.

Between each measurement, the Au thin film was subjected to a 1 min H_2:N_2 (5:95) plasma cleaning step, which removed all organic material from the surface. This procedure was preceded and followed by a thorough water rinse and yielded extremely clean Au surfaces, where baselines collected between two consecutive runs overlapped (see raw data collected over three cycles of adsorption/desorption in the Supporting Information). In contrast, cleaning the Au substrates using UV-ozone with exposure time of 5 min caused a morphology change to the surface, where the roughened film became more conductive with time. A comparison in Au film resistivity using both cleaning methods, upon repeated cycles of thiol adsorption/desorption, is presented in the Supporting Information. The glass cell and the glass stirrer bar were cleaned using UV-ozone.

RESULTS AND DISCUSSION

Resistivity and Monolayer Coverage. The thiols and disulfides used, summarized in Scheme 1, were selected to compare thiol versus disulfide adsorption kinetics and coverage, and the effect of charge on assembly. Chromatographic methods were developed (Supporting Information) to verify the absence of thiol in disulfides and the absence of disulfides in thiols (the latter

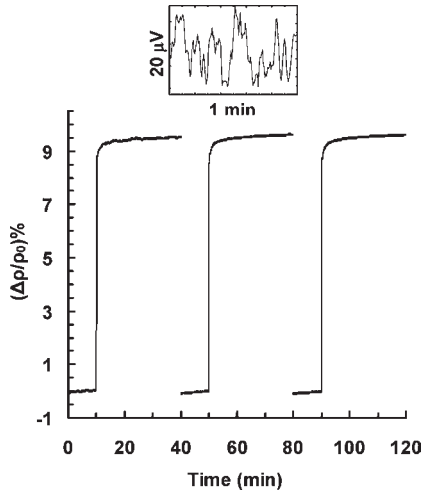

Figure 1. Adsorption of 0.2 mM $OH(CH_2)_2SH$ onto a clean Au thin film (7 mm × 2 mm x 14 nm): 10 min of collection in ultrapure water, followed by 30 min of the thiol monolayer formation. Three consecutive runs. Inset shows a detail for the signal at the plateau value.

is more likely due to slow air oxidation of thiols). High-purity thiol salts were produced by titrating the sulfonic acid with high purity metal hydroxides.

These small, water-soluble molecules can serve as building blocks for functionalizing surfaces, via ester or amide bonding with the hydroxyl- and carboxylate-terminated short chain SAMs for optical immunosensing applications.[21] Au electrodes modified with short chain negatively charged SAMs can selectively detect dopamine in the presence of organic interferents[22] or are used in biofuel cells.[23] Short chain zwitterionic thiols yield highly stable Au surfaces which resist the nonspecific adsorption of proteins and polymers for drug delivery and catalysis applications.[24] The chains are sufficiently short to prevent micellization at the concentrations used.

Thiols and disulfides chemisorb on clean gold with respective free energies ($\Delta G°$) of about −6 and −14 kcal per RS^- (eqs 1 and 2).[10b,25] The strong Au−S interaction of about −40 kcal contributes significantly to the net negative free energy. When the sulfur binds to a clean thin gold film, the resistance increases. We define $\Delta\rho$ as the difference between the resistivity of the bulk metal at time t (ρ) and the resistivity of the clean metal film at t_0 (ρ_0). Figure 1 shows three consecutive adsorption experiments of 0.2 mM $OH(CH_2)_2SH$ onto a 14 nm Au film from solution under constant stirring. The data are presented as the percentage of change in film resistivity ($\Delta\rho/\rho_0$%) versus time.

Theoretical work has shown that the resistivity change for Au thin films is linearly dependent on the amount and extent of electronic interaction between adsorbates and the substrate (thickness between 5 and 80 nm).[12] Persson[26] used a Newns−Anderson model to correlate the change in film resistivity to the mass (M), number density (n_a), and the vibrational damping rate ($1/\tau$) of scattering centers on chemisorption (eq 3), where n and e are the electron number density and charge, respectively, and d is the Au film thickness.

$$\Delta\rho = \frac{Mn_a}{n^2e^2d\tau} \tag{3}$$

When thiols/disulfides couple to electron−hole pairs in the substrate, their translational vibration rate ($1/\tau$) is dampened. This parameter varies linearly with the adsorbate density of states at the Fermi energy, $N(E_F)$, or the extent of electronic interaction between the thiols and the Au film (eq 4).

$$\frac{1}{\tau} = \frac{2m\omega_F\Gamma}{M}N(E_F)\langle\sin^2\theta\rangle \tag{4}$$

In eq 4, m is the electron mass, $\hbar\omega_F$ is the Fermi energy, Γ is the width of the adsorbate density of states, and $\langle\sin^2\theta\rangle$ is a geometric factor that depends on the orbital symmetry of the adsorbate molecular orbital near E_F. For a particular metal and adsorbate, with constant film thickness only n_a varies and $\Delta\rho$ is thus proportional to the number density.[12,26] Zhang et al. verified this proportionality using the adsorption of n-alkanethiolates on Au and an independent analytical method (SPR).[12a,b]

As seen in Figure 1, the runs are extremely reproducible. The signal-to-noise ratio was found to be ~600, which corresponds to a detection limit of 0.24% of a monolayer. In fact, most of the noise came from the stir bar. At saturation coverage, the variability between the three runs was found to be 0.3% as analyzed in the Supporting Information.

As expected, reproducibility and stability of the readings were critically dependent on cleaning. However, the use of UV-ozone, reported previously,[27] was found to be inferior to a hydrogen plasma in this respect. The most sensitive and telling indicator of surface cleanliness was a stable baseline prior to introduction of the adsorbant. UV-ozone cleaning gold gave adsorption profiles that were somewhat reproducible in $\Delta\rho$, but did not return to the starting ρ after each cleaning in addition to sloping baselines (examples in the Supporting Information). Repeated runs with the plasma treatment give the same starting resistance, showing no Au was lost due to etching or partial dissolution.

The four-probe resistivity measurements detect thiol adsorption in a geometric area of 2 mm × 7.5 mm. In order to estimate the actual surface area available for chemisorption, the surface roughness factor (defined as real/geometric surface area) was measured by reducing an oxide layer on the Au film.[28] The Supporting Information shows the cyclic voltammograms from which a roughness value of 1.17 was calculated. The thiol monolayer coverage was then determined using the reductive desorption method.[29] These measurements, presented in detail in the Supporting Information, show that $SH(CH_2)_2OH$ molecules pack at 4.47×10^{-10} mol cm^{-2} which corresponds to 57.6% of the theoretical value for the densely packed SAM of n-alkanethiol on Au(111).[1d,30a−30d] $[HS(CH_2)_2SO_3^-]_2Ca^{2+}$ molecules adsorb at 3.86×10^{-10} mol cm^{-2}, forming 49.7% of a densely packed monolayer. The measured coverage values are close to those previously reported for short-chain thiols adsorbed from aqueous solutions onto Au(111), where Calvente et al.[29c] determined a coverage for MESA of 3.8×10^{-10} mol cm^{-2}. The full monolayer in these aqueous, short-thiol systems is about half the coverage of a close-packed thiol SAM on Au due to disorder and enhanced tail repulsion from hydration and size (e.g., see Scheme 5 below).

Figure 2 shows how the rate and extent of adsorption vary with the thiol (A) and disulfide (B) concentrations. The assembly kinetics of $OH(CH_2)_2SH$ and $(OH(CH_2)_2S)_2$ was monitored while varying the concentrations by 2 orders of magnitude, from 2 to 200 μM and 1 to 100 μM, respectively. MESH contamination with the respective disulfide, examined using reversed-phase liquid chromatography (Figure S2, Supporting Information), verified that MESH solutions were almost free (less than 1.5%)

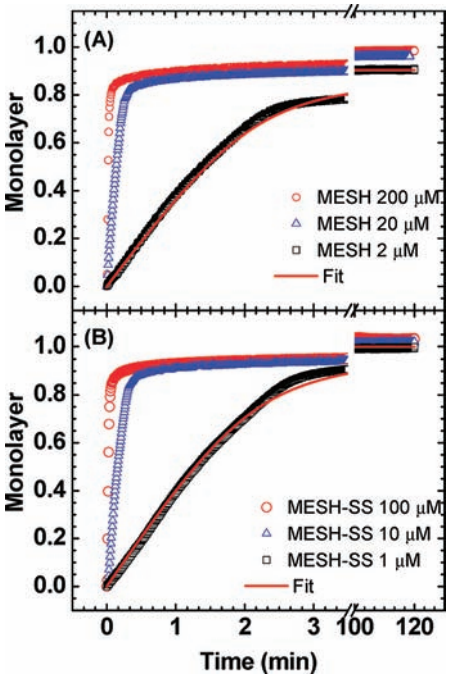

Figure 2. Adsorption kinetics of $OH(CH_2)_2SH$ (A) and $(OH(CH_2)_2S)_2$ (B) at a −S− concentration of 200 (red circle), 20 (blue triangle), and 2 (black square) μM onto the Au thin film (7.5 mm × 2 mm × 14 nm). The solid red line corresponds to the fit of the kinetic profile at the lowest concentration according to the model described in eq 12. Values of coverage are presented as fractions of a "full" monolayer, where the thiolate monolayer value corresponds to 4.61×10^{-10} mol cm^{-2} which is the highest coverage observed and where the adsorbed amount of thiolates is independent of concentration.

of any MESH-SS contaminants even 6 h after preparation and in contact with air. $\Delta\rho/\rho_0$ % values were converted into monolayer fraction and plotted versus time.

Adsorption profiles in Figure 2 show almost linear behavior with time for most of the adsorption, with a distinct slowdown at greater than about 80% of a monolayer. Steady-state values were obtained at longer times. The fact that the steady-state coverage was independent of solution concentration (at least for the disulfide) was taken as evidence that the systems are operating at the plateau (i.e., "full" monolayer regime) of the adsorption isotherm. In other words, at long time, the coverage reaches a "full" monolayer. This assumption is supported by calculations described below. The "full" monolayer coverage was 4.61×10^{-10} mol cm^{-2}. The assembly is presented on a log scale in Supporting Information (Figure S7). The fact that the lowest concentration of thiol does not reach the same coverage is significant and discussed later.

Well-Defined Mass Transport. The rate of adsorption is limited by a combination of resistance to mass transport to the surface and reaction kinetics at the solid−liquid interface (Langmuir kinetics). It is necessary to define and control at least one of these limiting mechanisms in order to deduce the other. It would appear straightforward to perform adsorptions in quiescent (unstirred) solutions and assume that mass transport will be limited by solution diffusion to the surface. Of course, there are other diffusional transport mechanisms, such as diffusion in two dimensions on the surface of the electrode during a possible "rearrangement" step, but such a step occurs only after the molecule has arrived at, and adsorbed to, the surface. Diffusion

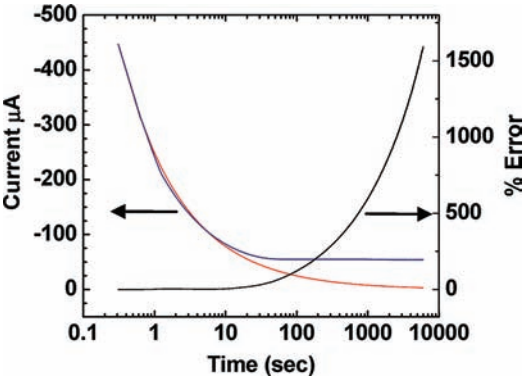

Figure 3. Chronoamperogram of potassium ferricyanide (10 mM) in 100 mM NaCl, at 129 mV vs SCE. Current was recorded at a Pt button electrode (0.20 cm^2) at 20 °C, under an Ar blanket. The blue line represents the measured current, the red line represents the current as predicted by the Cottrell model, and the black line represents the % error.

limited transport is characterized by a surface excess that initially increases as $t^{1/2}$. Here, we demonstrate the fallacy of assuming solution diffusion operates over long times.

Solution diffusion coefficients for ferricyanide were measured via cyclic voltammetry at the gold electrode. Following classical treatments,[31] the peak currents provided an accurate diffusion coefficient for ferricyanide of 5.23×10^{-6} cm^2 s^{-1} (for more detail, see the Supporting Information). The potentiostat was then reconfigured for a potential step experiment, where transport to the electrode (i.e., current) is limited to the diffusion controlled rate. In order to reduce convection currents to their minimum, the gold electrode was replaced by a platinum button electrode facing down, close to the bottom of the cell. Current, i versus time, for a quiescent solution, is presented in Figure 3. Also shown is the expected current versus time, as given by the Cottrell equation, where $i \sim t^{-1/2}$. Significant deviation is seen from diffusion controlled behavior *after less than a minute*. To emphasize this finding, the current was recorded up to 1 h and the % error, or difference, between diffusional behavior and the actual current presented in Figure 3. Clearly, assuming diffusion controlled transport beyond about a minute is unwarranted. The deviation is caused by convection currents from thermal gradients and vibrations, a fact well-known to electrochemists.[31]

Steady State Convective-Diffusion Mass Transport. As shown above, for typical thiol adsorption experiments, it is not possible to maintain mass transfer by diffusion alone beyond about a minute. Convective-diffusion, C-D, is steady state mass transport where convection, for example, by stirring or flowing the solution, sets up a constant diffusion layer of thickness δ. Flowing systems have been used frequently in monitoring SAM assemblies.[12,18,32] Camillone,[18] in particular, remarked on the difference in adsorption kinetics with flow rate, estimated rough adsorption times, and concluded the adsorption kinetics are diffusion limited, as did we from rough calculations.[10b]

In C-D, the flux of molecules to the surface (J_{RSH}, mol cm^{-2} s^{-1}), independent of time, is given by eq 5. The coverage (Γ, mol cm^{-2}) varies linearly with time where k_2 is the heterogeneous mass transport rate constant (1.7×10^{-3} cm s^{-1} under our experimental conditions) and C_b is the bulk concentration (mol cm^{-3}) of adsorbate

$$J_{RSH} = \frac{d\Gamma}{dt} = -k_2 C_b \rightarrow \Gamma = -k_2 C_b t \qquad (5)$$

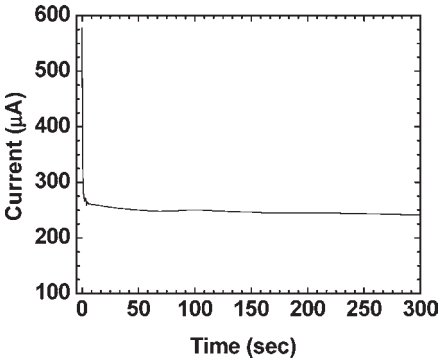

Figure 4. Chronoamperogram of MESH (10 mM) in NaCl (100 mM) at +675 mV vs Ag/AgCl, under stirring, at 20 °C and a collection rate of 2 Hz. $|i_l$ (MESH)$|$ = 247 μA for an exposed geometric surface area of 0.13 cm^2.

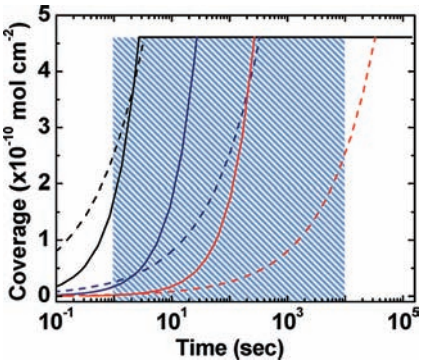

Figure 5. Model of thiol coverage as a function of time, at 100 (black lines), 10 (blue lines), and 1 (red lines) μM solution concentration. No Langmuir adsorption kinetics are present. The dashed lines represent the coverage based on a pure diffusion mechanism for a diffusion coefficient of 5×10^{-6} cm^{-2} s^{-1}, and the solid lines represent the coverage in the case of convective-diffusion mass transport with rate constant 1.7×10^{-3} cm s^{-1}. The plateau coverage value corresponds to a "full" monolayer. The shaded area represents the accessible time frame for our experiments, which ranges from about 1 s (limited by the mixing time) to almost 10^4 s. Using $\delta = (2D_{RSH}t)^{1/2}$, it takes about 1 s for species to cross the 34 μm diffusion layer (see the Supporting Information).

To determine k_2 for the thiols, electrochemical studies were performed on MESH and MESA-Ca solutions, in the adsorption reaction vessel, under identical experimental conditions, using the same Au surface as used for adsorption kinetics measurements. The Au film was masked off to expose only the section between the two inner conductivity electrodes, serving as the working electrode. The counter electrode was a platinum foil pressed against the sides of vessel walls so as not to interfere with the flux. The tip of the Ag/AgCl reference electrode was dipped in the solution behind the working electrode for minimal effect on the flux. MESH (Figure 4) and MESA-Ca were oxidized at 675 mV at 20 °C and at the same stirring rate as in adsorption kinetics experiments using 0.1 M NaCl as a supporting electrolyte. Figure 4 shows the expected steady-state current versus time for thiol oxidation from which an accurate k_2 is given directly. Additional details are presented in the Supporting Information.

Assuming a k_2 value of 1.7×10^{-3} cm s^{-1} and a "full" monolayer coverage of 4.6×10^{-10} mol cm^{-2}, the coverage versus time under C-D control for various solution concentrations can be estimated as in Figure 5. The data are presented in semilog format to compress the time axis. The coverage increases linearly with time and stops as soon as a "full" monolayer is attained.

For comparison, the expected coverage versus time for diffusion limited mass transport is also presented in Figure 5 under the same assumptions. Coverage varies as a function of the square root of time as shown in eq 6:[10b]

$$\Gamma = \frac{2D_{RSH}{}^{1/2}C_b t^{1/2}}{\pi^{1/2}} \qquad (6)$$

Using an estimate of $D_{RSH} \sim 5 \times 10^{-6}$ cm^{-2} s^{-1}, the dashed lines in Figure 5 show the expected coverage profiles for C_b = 1, 10, and 100×10^{-9} mol cm^{-3}.

The range of accessible times is from about 1 s, corresponding to the mixing time and the time it takes species to cross the 34 μm diffusion layer, to about 10^4 s. In this range, C-D is faster than diffusion alone and therefore would press Langmuir kinetics harder. Referring to the highest thiol concentration (0.1 mM) in the model described by Figure 5, it is clear that, using typical thiol concentrations of about 1 mM, any adsorption that is concluded to be limited by solution diffusion should be over in less than 10 s whether the solution is stirred or not.

Film Formation Kinetics. *Mass Transport Limited Rate.* The maximum possible rate would be limited only by mass transport. In C-D transport, a stagnant diffusion boundary layer is envisaged with thickness δ. This is a barrier across which molecules move solely by diffusion. At any distance x from the surface, for $x > \delta$, the concentration of adsorbate equals the bulk concentration, C_b. Under C-D limited transport, the concentration at $x = 0$ (the surface concentration, C_s) is zero with a linear concentration gradient from $0 < x < \delta$ (see the Supporting Information for a diagram). In this case, molecules arrive at the surface at their maximum rate ($d\Gamma_{max}/dt$) as defined in eq 7. Each molecule sticks to the surface (no limitations from Langmuir kinetics).

$$\frac{d\Gamma}{dt}(\max) = k_2 C_b = K_2 \qquad (7)$$

Film formation kinetics depend on the C-D limited rate constant (k_2) and on the thiol bulk concentration (C_b). For a given experiment, the bulk concentration may be assumed to be constant and included in the rate constant, K_2. k_2 values were measured for MESH and MESA-Ca using electrochemical oxidation as in Figure 4. The disulfides could not be oxidized (they are already oxidized), and MESA, MESA-Na, and MESA-Cs exhibited some (interesting but beyond the scope of this work) kinetically irreversible electrochemistry. Thus, k_2 values for the disulfides were approximated by those for the corresponding thiols and those for the salts by MESA-Ca, as summarized in Table 1.

Langmuir Kinetics. In the following analysis, it is assumed that the desorption rate is negligible. This assumption is justified if one is on the plateau of the adsorption isotherm, which is the case for all the systems except the lowest concentration of MESH, discussed in greater length below. In fact, we have shown that partial desorption occurs, but is on the time scale of several days.[10b]

a. K_1 Independent of Coverage. In Langmuir kinetics, the adsorption rate depends on the solution concentration and the number of available sites on the surface. In eq 8, k_1 is the Langmuir adsorption rate constant (cm s^{-1}) and C_s is the concentration *at the surface*. $1 - \Gamma$ is the fraction of available sites when coverage, Γ, is given in fractions of a monolayer. K_1 is the

Table 1. Values of Monolayer Coverage (mol cm^{-2}), Thiol/Disulfide Flux across the Hydrodynamic Diffusion Layer Barrier (mol cm^{-2} s^{-1}), Calculated Diffusion Coefficients (cm^2 s^{-1}) for Different Thiols/Disulfides, and Mass Transport Rate Constants (monolayer s^{-1}), at a Thiolate Concentration of 2 μM for R−SH and 1 μM for R−S−S−R

thiol/disulfide	monolayer coverage ($\times 10^{-10}$ mol cm^{-2})	flux of thiolate molecules at 2 μM −S− (J, $\times 10^{-12}$ mol cm^{-2} s^{-1})	diffusion coefficient (D_{20}, $\times 10^{-6}$ cm^2 s^{-1})	mass transport rate constant (monolayer s^{-1})
$HS(CH_2)_2OH$[a]	4.24	4.04	6.88	7.52
$(HO(CH_2)_2S)_2$[b]	4.61	4.04	6.88	7.52
$[HS(CH_2)_2SO_3^-]H^+$[b]	3.63	3.71	6.32	6.89
$[HS(CH_2)_2SO_3^-]Na^+$[b]	3.65	3.71	6.32	6.89
$[HS(CH_2)_2SO_3^-]Cs^+$[b]	3.86	3.71	6.32	6.89
$[HS(CH_2)_2SO_3^-]_2Ca^{2+}$[a]	3.86	3.71	6.32	6.89
$Fe(CN)_6^{3-}$	n/a	3.07	5.23	n/a

[a] Values are obtained by reductive desorption measurements and chronoamperometric data. [b] Values calculated using the results indicated by footnote *a*.

product of k_1 and C_s.

$$\frac{d\Gamma}{dt} = K_1(1-\Gamma) = k_1 C_s(1-\Gamma) \quad (8)$$

b. K_1 Dependent on Coverage. As with all studies on SAM formation, the adsorption kinetics for species studied here were observed to slow down significantly as the coverage approached its equilibrium value. For long-chain alkanethiols, it is generally believed that the significantly slower step that is observed after about half a monolayer has adsorbed represents various surface-localized rearrangements, ranging from "lying down" to "standing up" transitions, to packing of alkane chain tails. The neutral adsorbers investigated here show a "cleaner" profile, with the strong slowdown observed only after about 80% of the monolayer has formed. It is possible that, because of the short chains, the standing-up transition, if the molecules were lying down to begin with, is faster. Nevertheless, additional kinetic barriers exist at close to a "full" monolayer, which may reflect steric crowding around the remaining sites. The effect is captured by a k_1 value that decreases as coverage increases. Such a change may be modeled by any one of many additional factors, such as decreasing "sticking coefficients".[33] In the present case, we describe the rate constant by

$$k_1 = k_0(1-\Gamma) \quad (9)$$

where k_0 is the Langmuir rate constant unperturbed by lateral interaction, crowding, ordering, or standing up. Equation 9 is one of the simplest representations of how rate constant decreases with coverage. More complex dependences of k_1 on coverage are possible, including higher-order terms, which would improve the quality of fits to the experimental data. It is clear that at low coverage $k_1 \rightarrow k_0$, emphasizing the need to be able to make kinetic measurements at low Γ. Thus,

$$\frac{d\Gamma}{dt} = k_0 C_s(1-\Gamma)^2 \quad (10)$$

Langmuir Convective-Diffusion Kinetics. In the case of a convective diffusion system, which is present in our kinetic studies, the concentration of thiols at the Au surface (C_s, mol cm^{-3}) can be expressed in terms of the bulk concentration of thiols (C_b, mol cm^{-3}) according to eq 11. Figure S13 (Supporting Information) shows the concentration profile progression with time for a convective diffusion system. The SAM literature usually assumes that the surface concentration is the same as the bulk concentration. This is only true if the system has no mass transport limitations, as is the case of profile D in the Supporting Information. C_s is related to C_b according to the following:

$$C_s = C_b\left(1 - \frac{\frac{d\Gamma}{dt}}{\frac{d\Gamma}{dt}_{max}}\right) = C_b\left(1 - \frac{\frac{d\Gamma}{dt}}{k_2 C_b}\right) \quad (11)$$

After substituting C_s from eq 11 into eq 10, the net adsorption equation becomes

$$\frac{d\Gamma}{dt} = \frac{K_1(1-\Gamma)^2}{1 + \frac{K_1}{K_2}(1-\Gamma)^2} \quad (12)$$

It is important to note that, whether K_1 depends on coverage or not, the slopes at initial adsorption stages (low coverage, eq 13) are independent of the complexity that arises at higher coverage (nominally >50%).

$$\text{As } \Gamma \rightarrow 0, \quad \frac{d\Gamma_0}{dt} = \frac{K_1}{1 + \frac{K_1}{K_2}} \quad (13)$$

Equation 13 may be used for a critical analysis of some assumptions in the literature, which assumes self-assembly to be governed by Langmuir kinetics *or* mass transport. If the mass transport is steady state, both mechanisms initially depend linearly on solution concentration (compare eqs 7 and 8) and thus a plot of rate versus concentration *cannot tell them apart*. An independent measure of one mechanism, such as the electrochemical experiment in Figure 4, is required. Equation 13 shows clearly that if mass transport is limiting (K_2 small), both K_1 and K_2 will control the rate, but if surface reaction kinetics (Langmuir kinetics) is limiting (K_1 small) only K_1 will control the rate. In other words, *all* mass transport limited systems *must also* have a reaction limited component as well. This is because mass transport limitations lower the concentration of reagents at the surface (i.e., produce a concentration profile).

In modeling the experimental kinetics data, K_2 values determined from electrochemical measurements were used. K_1, which is the only parameter to fit, was determined from the best fits to the data according to eq 12. Figure 6 shows an example of how well the model fits to the whole adsorption profile range for the disulfide. The time progress of MESH-SS film formation from 1 μM solution is displayed, along with the fit to eq 12. The mass

transport and Langmuir rate constant values used are presented in Table 3.

Concentration Dependent Kinetics. In Figure 2A, the kinetic profiles of MESH are displayed for a range of concentrations (2, 20, and 200 μM). The data, plotted as a fraction of a monolayer versus time, are fit according to eq 12 (Table 2). The initial formation rate ($d\Gamma_0/dt$) was calculated at each concentration. The mass transport rate constant (K_2, monolayer s^{-1} and k_2, cm s^{-1}) is given from the electrochemical measurements of flux. Langmuir rate constant values (K_1, monolayer s^{-1} and k_0, cm s^{-1}) were then determined according to the best fits given by the proposed model. The fit at 2 μM is presented in Figure 2A. As seen in Table 2, when the concentration increases, the initial formation rate ($d\Gamma_0/dt$) increases by the same factor.

At initial stages of film formation, up to 80% of final coverage, the amount of adsorbed thiolates varies linearly with time, suggesting fast adsorption kinetics. The slopes at initial increase ($d\Gamma_0/dt$) for different concentrations are close to the rate of formation of a "full" monolayer based on a pure mass transport adsorption mechanism (K_2). This fact suggests that MESH adsorption is mainly governed by the mass transport of molecules toward the Au film, for up to 80% of SAM completion. Monolayer assemblies were monitored for up to 2 h, after which the change in resistivity was negligible and approached the baseline drift before the start of the experiment, interpreted to show that a "full" monolayer forms well within 2 h.

Kinetics of Adsorption of Thiols versus the Respective Disulfides. Figure 7 shows a direct comparison between the film assembly of MESH and MESH-SS at the lowest −S− concentration (2 μM MESH and 1 μM MESH-SS). A comparison of 20/10 μM MESH/MESH-SS is provided in the Supporting Information. While higher-concentration thiol versus disulfide samples show almost identical kinetics over the whole range, the more dilute samples differed slightly but consistently at higher coverage. In Figure 7, the kinetic profiles indicate, for up to 80% of film completion, the thiol and disulfide adsorb at the same rates (Table 3; initial formation rate).

The concentration of disulfide was one-half that of the thiol, assuming the diffusion coefficients to be the same. If this assumption holds, MESH-SS and MESH cross the diffusion layer barrier and reach the Au surface at the same rate. Then both thiol and disulfide are able to (i) displace water molecules off of the Au surface; (ii) physisorb; (iii) find one available adsorption site (for the thiol) or two available adjacent sites (for the disulfide); (iv) dissociate (S−H or S−S homolytic bond cleavage; and (v) interact with the Au film surface, all at the same rate. If the foregoing were true, it would imply that the S−H bond dissociation upon chemisorption is not the rate limiting step, nor is the S−S bond reduction, unless they happen at exactly the same rate.

MESH-SS attaches randomly to the surface when two vacant adjacent sites are available, leading to the formation of isolated empty sites on the Au film. As time progresses and the SAM forms, the probability of finding a pair of adjacent empty sites decreases. Interestingly, the fact that MESH-SS still adsorbs at the same rate as that of MESH even at higher coverage suggests that the thiolates are able to rapidly diffuse on the surface, filling up the isolated empty sites and allowing additional S−S molecules to incorporate. The high-coverage assembly of thiol versus disulfide may be compared with the random sequential model.[34] This model considers the adsorbing molecules to be hard spheres, which hit and stick to a surface without migration.

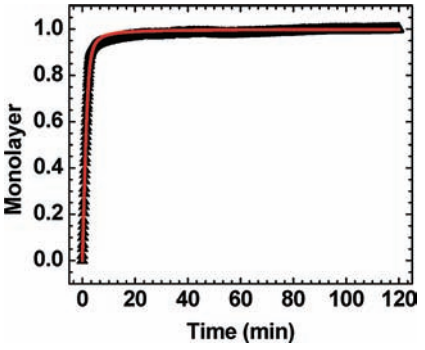

Figure 6. Progress of MESH-SS film formation from 1 μM solution onto the Au thin film (7.5 mm × 2 mm × 14 nm). (black triangle) Experimental data as a fraction of a monolayer; (solid red line) fit from the model presented in eq 12. The actual monolayer value corresponds to 4.61×10^{-10} mol cm^{-2}.

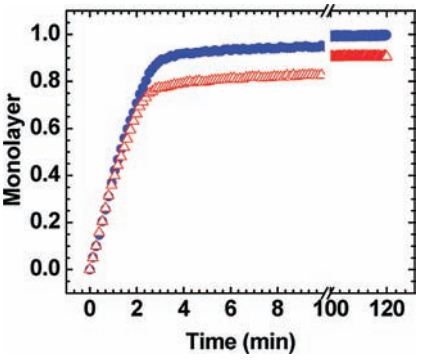

Figure 7. Comparison plot of MESH-SS (blue circle) and MESH (red triangle) film formation kinetics onto the Au thin film (7.5 mm × 2 mm × 14 nm) from 1 and 2 μM solutions, respectively. A "full" monolayer corresponds to 4.61×10^{-10} mol cm^{-2}.

Table 2. Concentration Dependent Kinetics of $OH(CH_2)_2S$/Au Film Formation[a]

		Langmuir rate constant		mass transport rate constant	
$[OH(CH_2)_2SH]$ M	initial formation rate, $d\Gamma_0/dt$ (monolayer s^{-1})	K_1 (monolayer s^{-1})	k_0 ($\times 10^{-3}$ cm s^{-1})	K_2 (monolayer s^{-1})	k_2 ($\times 10^{-3}$ cm s^{-1})
2×10^{-4}	0.58	2.5	5.6	0.752	1.73
2×10^{-5}	0.057	0.24	5.6	0.0752	1.73
2×10^{-6}	0.0064	0.067	15	0.00752	1.73

[a] $d\Gamma_0/dt$ values correspond to the slopes of the experimental kinetics data at initial adsorption. Langmuir rate constants are based on the best fits provided by eq 12. Mass transport rate constants are determined using electrochemical measurements. Errors for K_2 and k_2 are ±2%, and errors for K_1 and k_1 are ±20%.

Table 3. Rate Constant Values Used to Model the Kinetics Experimental Data According to eq 12

		Langmuir rate constant		mass transport rate constant	
thiol/disulfide	Initial formation rate, $d\Gamma_0/dt$ ($\times 10^{-3}$ cm s^{-1})	K_1 ($\times 10^{-2}$ monolayer s^{-1})	k_0 ($\times 10^{-3}$ cm s^{-1})	K_2 ($\times 10^{-3}$ monolayer s^{-1})	k_2 ($\times 10^{-3}$ cm s^{-1})
$HS(CH_2)_2OH$	1.49	6.7	15	7.52	1.73
$(HO(CH_2)_2S)_2$	1.50	7.0	16	7.52	1.73
$[HS(CH_2)_2SO_3^-]H^+$	1.22	2.2	5.1	6.89	1.59
$[HS(CH_2)_2SO_3^-]Na^+$	1.22	2.3	5.2	6.89	1.59
$[HS(CH_2)_2SO_3^-]Cs^+$	1.21	2.2	5.1	6.89	1.59
$[HS(CH_2)_2SO_3^-]_2Ca^{2+}$	1.22	2.3	5.3	6.89	1.59

A jamming limit is defined in the case of dimers (i.e., disulfide adsorption), where the probability of incorporating an additional particle to the film approaches zero after all adjacent sites are taken up. This jamming limit is 0.91 for a square lattice and 0.915 for a hexagonal lattice.[34d] In other words, if the disulfide does not move upon chemisorption, it can only cover 91% of the surface area covered by the respective thiol. It must be concluded that the diffusion of thiolate molecules on the surface occurs with sufficient speed so as not to limit the disulfide adsorption rate.

For diffusion on a planar surface via a site-to-site hopping mechanism, the diffusion coefficient, $D_{surface}$, can be determined from the mean-square of the hopping distance, $\langle X^2 \rangle$, and the hopping time, t, of the thiolate, according to the following equation:[35]

$$D_{surface} = \frac{\langle X^2 \rangle}{4t} \qquad (14)$$

We cannot measure surface diffusion coefficients, but we can estimate a lower limit assuming surface-attached species must be able to diffuse faster than unbound species arriving at the surface. For 0.2 mM experiments, disulfide arrives at the rate of about 1 monolayer s^{-1}, or 2.4 $\times$ 10^{14} sulfurs cm^{-2} s^{-1}. The distance between molecules at this coverage is 6.4 Å and the minimum value for $D_{surface}$ is about 10^{-15} cm^2 s^{-1} (at 20 °C) for a hopping time of <1 s. Diffusion of chemisorbed thiolate chains on gold surfaces has been the subject of many investigations.[36] Our value is many orders of magnitude faster than those estimated for long-chain alkane thiols on Au (for example, $D_{surface} \sim 10^{-18}$ cm^2 s^{-1} at 60 °C[36c]). Because of the strong binding energy between Au atoms and S head groups, it has been suggested the diffusion energy barrier for long-chain thiolates is higher than that for a Au−thiolate complex on the surface.[36a,e] Therefore, the transport of adsorbates on the surface is believed to be accompanied by the movement of gold atoms underneath the SAM.[36a,d]

The fact that they are disordered[37] and (50%) less densely packed could be one major contributor to the faster diffusion of short-chain thiolates. It is known that the lateral diffusion of molecules is reduced by lateral interactions of the organic layer.[36a] It is concluded that surface mobility of a substrate atom−adsorbate complex leads to the formation of etch pits on the Au film surface.[36d] We find no evidence for etching in our thin films. For example, the change in the resistance for a Au film was monitored over 25 cycles of thiol adsorption/desorption. The resistance increased by less than 0.03%/cycle (see the Supporting Information). The conductivity of the Au thin film under investigation (14 nm thick) is 86 000 Ω^{-1} cm^{-1}. This value corresponds to 54.5 Au sheets (taking into account the film thickness, d_{Au}= 19.3 and M_w of 196.7 g mol^{-1}). The loss in conductivity of the film/cycle thus corresponds to a loss of a submonolayer of Au atoms (0.016 Au monolayer/cycle) at most.

Scheme 2. Proposed "Disulfide Walking" Mechanism for Surface Diffusion of Thiolates on Au

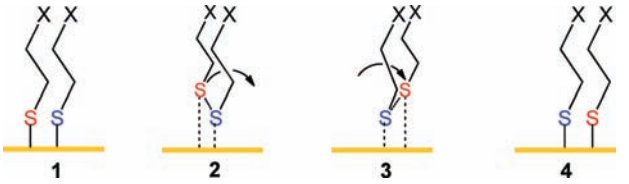

Scheme 3. Adsorption via Thiol and Desorption as Disulfide

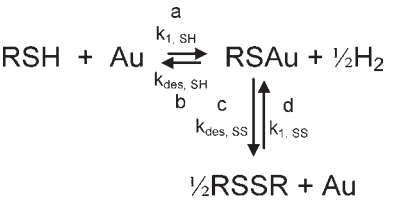

Scheme 4. Rate Equations for Thiol and Disulfide Adsorption/Desorption onto the Au Surface

a. $$\frac{d[RSAu]}{dt} = k_{1,SH}[RSH](1-\Gamma)$$

b. $$-\frac{d[RSAu]}{dt} = k_{des,SH}[H_2]^{1/2}\Gamma$$

c. $$-\frac{d[RSAu]}{dt} = k_{des,SS}\Gamma$$

d. $$\frac{d[RSAu]}{dt} = k_{1,SS}[RSSR]^{1/2}(1-\Gamma)$$

A possible mechanism for thiolate transport is shown in Scheme 2, which shows pivoting of one thiolate around another with an intermediate that has partial disulfide bond character. Full detachment in this "disulfide walking" model is not required in this mechanism, and is only possible with a disordered system with plenty of vacant Au surface atoms available, which is the case here.

dx.doi.org/10.1021/ja2041833 |J. Am. Chem. Soc. 2011, 133, 16080–16091

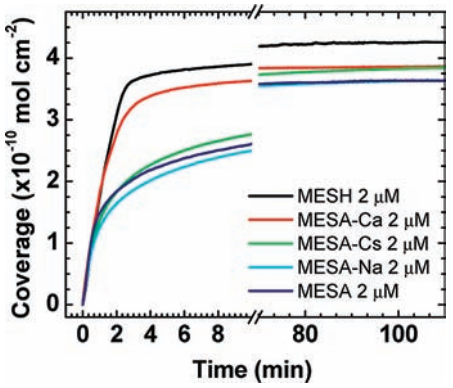

Figure 8. Progress of self-assembled monolayer formation of charged vs neutral thiols at a −S− concentration of 2 μM.

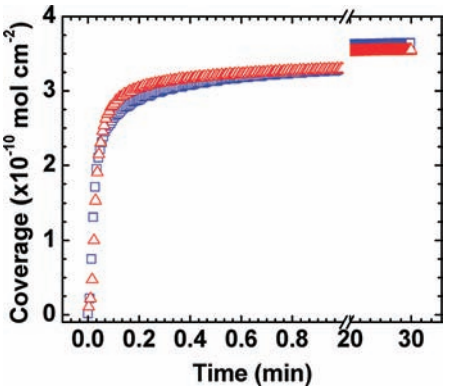

Figure 9. Assembly of MESA-Na from 0.2 mM solutions under charge screened (red triangle) and unscreened (blue square) conditions.

As seen in Figure 7, at the lowest thiol concentration (2 μM), the thiol coverage value is slightly lower than that of the disulfide. This finding may be explained by previous work,[10b] which found that thiolates can desorb as disulfides, as represented in Scheme 3.

Realizing [Au] = 1 − Γ and [RSAu] = Γ, the adsorption and desorption rate equations which apply for each step (a, b, c, and d) are presented in Scheme 4.

At initial adsorption stages (the linear regime, for up to 80% of film formation), in the case of MESH and MESH-SS adsorption, the initial formation rates are the same, $k_{1,SH} = k_{1,SS} = 15 \times 10^{-3}$ cm s^{-1}. For [H_2] = 0 and [RSSR] = 0 (i.e., no disulfide in the solution) at steady state, a *faux* or *apparent* equilibrium, described by a constant K_{app}, is observed:

$$k_{1,SH}[RSH](1-\Gamma) = k_{des,SS}\Gamma \quad (15)$$

$$K_{app} = \frac{k_{1,SH}}{k_{des,SS}} = \frac{\Gamma}{[RSH](1-\Gamma)} \quad (16)$$

that is, the rate of adsorption as *thiols* equals the rate of desorption as *disulfides*.

For [RSH] = 2×10^{-6} M and Γ = 0.92, $K_{app} = 5.8 \times 10^6$. Thus, the adsorption rate constant for the thiol ($k_{1,SH}$ from Table 3 = 15×10^{-3}) is 5.8×10^6 times larger than the desorption rate constant for disulfide, $k_{des,SS} = 2.6 \times 10^{-9}$ cm s^{-1}. Using

$$K_{SS} = \frac{\Gamma}{[RSSR]^{1/2}(1-\Gamma)} \quad (17)$$

the disulfide adsorption equilibrium constant, K_{SS}, is equal to 5.8×10^6. For [RSSR] = 1 μM, Γ is 0.9998 Γ_{max}, validating the assumption of a full monolayer under these conditions. $\Delta G^\circ_{ad,SS}$ is thus −38 kJ for 1/2 RSSR or −76 kJ/RSSR or −18 kcal. This value compares well with the net adsorption energy of didecyldisulfide reported by Kolega and Schlenoff (−14 kcal).[25]

Charged versus Neutral Thiols. To investigate the charge effect on the adsorption of water-soluble thiols, a negatively charged thiol, hydrogen 2-mercaptoethane sulfonate (MESA), having the same hydrocarbon chain length as the neutral MESH, was studied. The adsorption profiles from 2 μM solutions are presented in Figure 8. It is important to note that, for the charged thiols, even this low concentration falls on the Langmuir isotherm plateau (see the Supporting Information). A summary of the rate constants which yielded the best fit for the data according to eq 12 is presented in Table 3. The kinetics at initial adsorption stages for the MESH and MESA ($d\Gamma_0/dt$) are similar, since the assembly is limited mainly by the transport of species in solution. Nevertheless, the assembly of the sulfonated thiol starts slowing down considerably earlier compared to the alcohol terminated thiol and has lower k_1 values (Table 3).

Initially, one can rationalize the slower adsorption of (charged) MESA compared to the (neutral) MESH at higher coverage as a result of electrostatic repulsion between surface and incoming thiols for the former. This hypothesis was tested by comparing the assembly kinetics of sodium 2-mercaptoethane sulfonate, MESA-Na, at 0.2 mM in ultrapure water and in the presence of excess sodium perchlorate (2 mM). Perchlorate is a weakly adsorbing anion. The Debye screening length for MESA-Na at 0.2 mM is 21.5 nm.[38] This value decreases to 6.80 nm in 2 mM $NaClO_4$ (see the Supporting Information for calculations).[38] The comparison is presented in Figure 9, which reveals that similar adsorption rates and coverage values are obtained for the MESA-Na assembly with or without the added long-range screening afforded by excess salt ions.

Since long-range electrostatics are not responsible for slowing down adsorption, it is likely that short-range steric interactions may come into play, a reasonable thesis considering the greater bulk of the sulfonate tail group compared to −OH. The sulfonate group includes the counterion, and both MESA and MESH will be more hydrated than the short alkane (−C_2H_4−) midsection. MESA-Na and MESA-Cs diffuse toward the Au surface at the same rate and exhibit the same mechanism of attachment (similar initial adsorption rates, k_1, k_2 values in Table 3). It is evident from the adsorption profiles (Figure 8) and the rate constant values (Table 3) that changing the monovalent counterion has little effect on thiol assembly kinetics and extent for MESA, MESA-Na, and MESA-Cs, although there is a slight indication that the Cs^+ salt assembles fastest among the three monovalent cations and gives slightly higher coverages, being the least hydrated. A comparison of the hydration shell radius (Table S1, Supporting Information) would predict that MESA-H (H^+ hydrated radius 0.282 nm) might adsorb faster than MESA-Na (Na^+ radius 0.358 nm) or MESA-Cs (Cs^+ radius 0.329 nm) if kinetics were limited by counterion size. That this is not the case is probably attributable to the bulkiness of the sulfonate tail group (0.357 nm) which is as large as, or larger than, the counterions.

Scheme 5 provides a to-scale depiction of the relative sizes of the −OH and sulfonate tail groups. The experimental average intermolecular spacing is shown in Scheme 5, and the relative tail group sizes clearly suggest that the packing density observed is

Scheme 5. Representation of MESH (A) and MESA-Na (B) Molecules on the Au Film Surface[a]

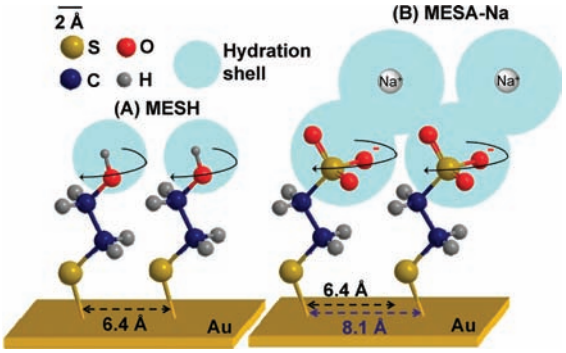

[a] Atom sizes, bond lengths, angles, hydration shells, and intermolecular spacing are to scale (numeric values are detailed in the Supporting Information). The slower adsorption rate of MESA-Na compared to MESH could be explained by the steric crowding caused by the bulkiness of the hydrated sulfonate groups. The distance between the adsorbates is determined from the final coverage values for each molecule, which were 3.63×10^{-10} mol cm^{-2} for MESA and 4.24×10^{-10} mol cm^{-2} for MESH.

Scheme 6. Representation of MESA-Na (A) and MESA-Ca (B) Assemblies on the Au Film Surface[a]

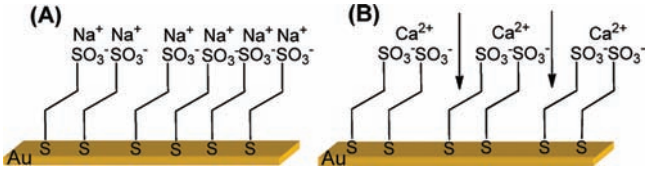

[a] The fact that each Ca^{2+} ion complexes with two MESA molecules, accompanied by a fast diffusion of adsorbed species on the surface, allows more compact organization of the latter, leading to a faster incorporation of additional adsorbates.

limited by steric interactions. Little order is expected from this system, leaving the adsorbed thiolates to rotate as shown. The question remains as to whether the slowdown after half a monolayer seen in Figure 8 could be caused by the lying down → standing up transition posited for long-chain alkanethiols. The lying-down phase, if it were to occur, would be more likely for the −OH system, since the bulk of the $-SO_3^-$ would present problems for a flat configuration. In either case, the two CH_2 units in the alkane chain would have minimal van der Waals interactions with the surface compared to long alkane chains. In a recent detailed study of the standing up transition, Calvente et al.[39] found that short-chain, hydrophilic thiolates reorient well below the saturation coverage of the lying down phase.

It is important to note that the monolayer coverage for the MESA did not change after 12 h of collection.

The film assembly dependence on the valence of the counterion was examined by studying the adsorption of calcium 2-mercaptoethane sulfonate (MESA-Ca). The results (Figure 8) show that MESA-Ca adsorbs initially at the same rate as the other charged thiols ($d\Gamma_0/dt$, Table 3), reaching the same final coverage. For the region between 40% and 90% of film formation, MESA-Ca adsorbs twice as fast as the other charged thiols. This is explained by two factors. The first could be the rising

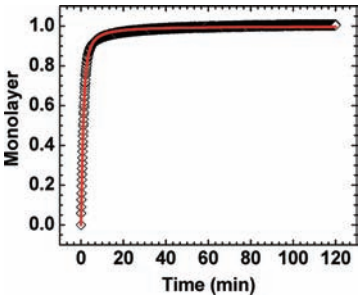

Figure 10. Progress of MESA-Ca film formation from 2 μM solution. (black diamonds) Experimental data as a fraction of a monolayer; (solid red line) fit from the model presented in eq 12. The actual monolayer value corresponds to 3.86×10^{-10} mol cm^{-2}.

and tilting of the chains which is happening at twice the rate compared to MESA with monovalent counterions. The fact that one cation exists for two thiol chains in the case of MESA-Ca renders the lying-down phase energetically less stable for entropic reasons. The entropic effect on accelerating SAM kinetics has been shown before when assembly is done in confined microenvironments compared to unconfined bare substrates,[40] where spatial confinement is thought to force the adsorbates into the standing up position directly, bypassing the lying-down configuration. Faster adsorption could also be caused by better organization and ordering of chains on the Au surface (Scheme 6), where Ca^{2+} orders two adjacent thiolates. This phenomenon is well-known in biology where the binding of Ca^{2+} to phospholipids in bilayers brings them into closer contact which leads to the ordering of phospholipid tails.[41] Figure 10 shows the assembly profile of MESA-Ca from 2 μM solution. The experimental data and fit (according to eq 12) are presented as a monolayer fraction versus time, where the actual monolayer value corresponds to 3.86×10^{-10} mol cm^{-2}.

CONCLUSIONS

An effort was made here to address three major challenges in SAM assembly of thiols/disulfides on gold: a defined rate of mass transport to the surface was maintained and measured over the entire adsorption experiment; ultraclean surfaces were produced; and a highly sensitive technique for measuring surface excess down to 0.1% of a monolayer was employed. In addition, complexity arising from long-term crystalline packing of alkane chain tails and lying down → standing up transitions was minimized with the use of short, hydrophilic thiols. The progress of adsorption can then be clearly and quantitatively broken down into limitations from mass transport and Langmuir adsorption kinetics. Individually, equations for C-D and Langmuir kinetics are both proportional to solution concentration, which may have led to some of the contradictions in the literature concerning mass transport versus Langmuir kinetic limitations on SAM assembly. An equation derived here shows how both are coupled and how mass transfer limitations impact Langmuir kinetics. The precision and accuracy afforded by the experimental techniques permit a head-to-head comparison of thiol versus disulfide adsorption kinetics, here shown to be the same, and charged versus neutral thiols, here shown to be limited by steric (or at least short-range) interactions rather than long-range electrostatic interactions.

■ ASSOCIATED CONTENT

Supporting Information. Experimental setup scheme, chromatographic separation data for MESH/Au surface roughness determination, reductive desorption of thiols, adsorbate flux measurements, electrochemical studies, adsorption kinetic profiles for various thiols and disulfides for long time scales. This material is available free of charge via the Internet at http://pubs.acs.org.

■ AUTHOR INFORMATION

Corresponding Author
schlen@chem.fsu.edu

■ REFERENCES

(1) (a) Nuzzo, R. G.; Zegarski, B. R.; Dubois, L. H. *J. Am. Chem. Soc.* **1987**, *109*, 733–740. (b) Nuzzo, R. G.; Fusco, F. A.; Allara, D. L. *J. Am. Chem. Soc.* **1987**, *109*, 2358–2368. (c) Bain, C. D.; Biebuyck, H. A.; Whitesides, G. M. *Langmuir* **1989**, *5*, 723–727. (d) Nuzzo, R. G.; Dubois, L. H.; Allara, D. L. *J. Am. Chem. Soc.* **1990**, *112*, 558–569. (e) Bryant, M. A.; Pemberton, J. E. *J. Am. Chem. Soc.* **1991**, *113*, 8284–8293. (f) Li, Y. Z.; Huang, J. Y.; McIver, R. T.; Hemminger, J. C. *J. Am. Chem. Soc.* **1992**, *114*, 2428–2432. (g) Biebuyck, H. A.; Whitesides, G. M. *Langmuir* **1993**, *9*, 1766–1770.

(2) (a) Whitesides, G. M.; Laibinis, P. E. *Langmuir* **1990**, *6*, 87–96. (b) Ulman, A. *Chem. Rev.* **1996**, *96*, 1533–1554. (c) Love, J. C.; Estroff, L. A.; Kriebel, J. K.; Nuzzo, R. G.; Whitesides, G. M. *Chem. Rev.* **2005**, *105*, 1103–1169. (d) Vericat, C.; Vela, M. E.; Salvarezza, R. C. *Phys. Chem. Chem. Phys.* **2005**, *7*, 3258–3268. (e) Kind, M.; Woell, C. *Prog. Surf. Sci.* **2009**, *84*, 230–278. (f) Vericat, C.; Vela, M. E.; Benitez, G.; Carro, P.; Salvarezza, R. C. *Chem. Soc. Rev.* **2010**, *39*, 1805–1834.

(3) (a) Sondaghuethorst, J. A. M.; Schonenberger, C.; Fokkink, L. G. J. *J. Phys. Chem.* **1994**, *98*, 6826–6834. (b) Schessler, H. M.; Karpovich, D. S.; Blanchard, G. J. *J. Am. Chem. Soc.* **1996**, *118*, 9645–9651. (c) Bensebaa, F.; Voicu, R.; Huron, L.; Ellis, T. H.; Kruus, E. *Langmuir* **1997**, *13*, 5335–5340. (d) Nagahara, T.; Suemasu, T.; Aida, M.; Ishibashi, T.-A. *Langmuir* **2010**, *26*, 389–396.

(4) (a) Buck, M.; Grunze, M.; Eisert, F.; Fischer, J.; Trager, F. *J. Vac. Sci. Technol., A* **1992**, *10*, 926–929. (b) Houssiau, L.; Bertrand, P. *Appl. Surf. Sci.* **2001**, *175−176*, 399–406. (c) Bieri, M.; Buergi, T. *Phys. Chem. Chem. Phys.* **2006**, *8*, 513–520. (d) Martinez, L.; Carrascosa, L. G.; Huttel, Y.; Lechuga, L. M.; Roman, E. *Phys. Chem. Chem. Phys.* **2010**, *12*, 3301–3308. (e) Valkenier, H.; Huisman, E. H.; van Hal, P. A.; de Leeuw, D. M.; Chiechi, R. C.; Hummelen, J. C. *J. Am. Chem. Soc.* **2011**, *133*, 4930–4939.

(5) (a) Bain, C. D.; Troughton, E. B.; Tao, Y. T.; Evall, J.; Whitesides, G. M.; Nuzzo, R. G. *J. Am. Chem. Soc.* **1989**, *111*, 321–335. (b) Kim, Y. T.; McCarley, R. L.; Bard, A. J. *Langmuir* **1993**, *9*, 1941–1944. (c) Garg, N.; Friedman, J. M.; Lee, T. R. *Langmuir* **2000**, *16*, 4266–4271.

(6) (a) Hahner, G.; Woll, C.; Buck, M.; Grunze, M. *Langmuir* **1993**, *9*, 1955–1958. (b) Peterlinz, K. A.; Georgiadis, R. *Langmuir* **1996**, *12*, 4731–4740.

(7) Schreiber, F. *J. Phys.: Condens. Matter* **2004**, *16*, R881–R900.

(8) (a) Karpovich, D. S.; Blanchard, G. J. *Langmuir* **1994**, *10*, 3315–3322. (b) Pan, W.; Durning, C. J.; Turro, N. J. *Langmuir* **1996**, *12*, 4469–4473. (c) Liao, S.; Shnidman, Y.; Ulman, A. *J. Am. Chem. Soc.* **2000**, *122*, 3688–3694. (d) Shen, D. Z.; Huang, M. H.; Chow, L. M.; Yang, M. S. *Sens. Actuators, B* **2001**, *77*, 664–670. (e) Bieri, M.; Buergi, T. *J. Phys. Chem. B* **2005**, *109*, 22476–22485. (f) Patton, D.; Knoll, W.; Advincula, R. C. *Macromol. Chem. Phys.* **2011**, *212*, 485–497.

(9) (a) Georgiadis, R.; Peterlinz, K. P.; Peterson, A. W. *J. Am. Chem. Soc.* **2000**, *122*, 3166–3173. (b) Damos, F. S.; Luz, R. C. S.; Kubota, L. T. *Langmuir* **2005**, *21*, 602–609. (c) Damos, F. S.; Luz, R. C. S.; Sabino, A. A.; Eberlin, M. N.; Pilli, R. A.; Kubota, L. T. *J. Electroanal. Chem.* **2007**, *601*, 181–193. (d) Jiang, G. Q.; Deng, S. X.; Baba, A.; Huang, C. Y.; Advincula, R. C. *Macromol. Chem. Phys.* **2010**, *211*, 2562–2572.

(10) (a) Zelenay, P.; Ricejackson, L. M.; Wieckowski, A. *Langmuir* **1990**, *6*, 974–979. (b) Schlenoff, J. B.; Li, M.; Ly, H. *J. Am. Chem. Soc.* **1995**, *117*, 12528–12536.

(11) Rubini, R. Q. The use of thin film conductance and surface analysis to characterize the chemisorption of organic thiols and disulfides on metal surfaces. Ph.D. Dissertation, University of South Florida, Tampa, FL, 1993.

(12) (a) Zhang, Y.; Terrill, R. H.; Bohn, P. W. *J. Am. Chem. Soc.* **1998**, *120*, 9969–9970. (b) Zhang, Y. M.; Terrill, R. H.; Bohn, P. W. *Anal. Chem.* **1999**, *71*, 119–125. (c) Fried, G. A.; Zhang, Y. M.; Bohn, P. W. *Thin Solid Films* **2001**, *401*, 171–178.

(13) (a) Venkataramanan, M.; Pradeep, T. *Chem. Phys. Lett.* **2000**, *327*, 299–304. (b) Venkataramanan, M.; Pradeep, T. *Anal. Chem.* **2000**, *72*, 5852–5856. (c) Pugmire, D. L.; Tarlov, M. J.; van Zee, R. D.; Naciri, J. *Langmuir* **2003**, *19*, 3720–3726. (d) Hung, D.; Liu, Z.; Shah, N.; Hao, Y. W.; Searson, P. C. *J. Phys. Chem. C* **2007**, *111*, 3308–3313.

(14) (a) Benitez, G.; Vericat, C.; Tanco, S.; Lenicov, F. R.; Castez, M. F.; Vela, A. E.; Salvarezza, R. C. *Langmuir* **2004**, *20*, 5030–5037. (b) Mokrani, C.; Fatisson, J.; Guerente, L.; Labbe, P. *Langmuir* **2005**, *21*, 4400–4409. (c) Saavedra, H. M.; Barbu, C. M.; Dameron, A. A.; Mullen, T. J.; Crespi, V. H.; Weiss, P. S. *J. Am. Chem. Soc.* **2007**, *129*, 10741–10746. (d) Kazakeviciene, B.; Valincius, G.; Niaura, G.; Talaikyte, Z.; Kazemekaite, M.; Razumas, V.; Plausinaitis, D.; Teiserskiene, A.; Lisauskas, V. *Langmuir* **2007**, *23*, 4965–4971. (e) Hohman, J. N.; Zhang, P. P.; Morin, E. I.; Han, P.; Kim, M.; Kurland, A. R.; McClanahan, P. D.; Balema, V. P.; Weiss, P. S. *ACS Nano* **2009**, *3*, 527–536. (f) Kim, M.; Hohman, J. N.; Morin, E. I.; Daniel, T. A.; Weiss, P. S. *J. Phys. Chem. A* **2009**, *113*, 3895–3903.

(15) Biebuyck, H. A.; Bian, C. D.; Whitesides, G. M. *Langmuir* **1994**, *10*, 1825–1831.

(16) (a) Jung, C.; Dannenberger, O.; Xu, Y.; Buck, M.; Grunze, M. *Langmuir* **1998**, *14*, 1103–1107. (b) Dannenberger, O.; Buck, M.; Grunze, M. *J. Phys. Chem. B* **1999**, *103*, 2202–2213. (c) Shon, Y.-S.; Lee, T. R. *J. Phys. Chem. B* **2000**, *104*, 8182–8191.

(17) (a) Vanderah, D. J.; Walker, M. L.; Rocco, M. A.; Rubinson, K. A. *Langmuir* **2008**, *24*, 826–829. (b) Walker, M. L.; Vanderah, D. J.; Rubinson, K. A. *Colloids Surf., B* **2011**, *82*, 450–455.

(18) Camillone, N. *Langmuir* **2004**, *20*, 1199–1206.

(19) (a) Porter, M. D.; Bright, T. B.; Allara, D. L.; Chidsey, C. E. D. *J. Am. Chem. Soc.* **1987**, *109*, 3559–3568. (b) DeBono, R. F.; Loucks, G. D.; DellaManna, D.; Krull, U. J. *Can. J. Chem.* **1996**, *74*, 677–688. (c) Dannenberger, O.; Wolff, J. J.; Buck, M. *Langmuir* **1998**, *14*, 4679–4682. (d) Shao, H. B.; Yu, H. Z.; Cheng, G. J.; Zhang, H. L.; Liu, Z. F. *Phys. Chem. Chem. Phys.* **1998**, *102*, 111–117. (e) Kang, J. F.; Zaccaro, J.; Ulman, A.; Myerson, A. *Langmuir* **2000**, *16*, 3791–3796. (f) Jakubowicz, A.; Jia, H.; Wallace, R. M.; Gnade, B. E. *Langmuir* **2005**, *21*, 950–955. (g) Campbell, C. J.; Fialkowski, M.; Bishop, K. J. M.; Grzybowski, B. A. *Langmuir* **2009**, *25*, 9–12. (h) Henderson, A. P.; Seetohul, L. N.; Dean, A. K.; Russell, P.; Pruneanu, S.; Ali, Z. *Langmuir* **2009**, *25*, 931–938.

(20) (a) Hu, K.; Bard, A. J. *Langmuir* **1998**, *14*, 4790–4794. (b) Bellino, M. G.; Calvo, E. J.; Gordillo, G. *Phys. Chem. Chem. Phys.* **2004**, *6*, 424–428. (c) Rooth, M.; Shaw, A. M. *J. Phys. Chem. C* **2007**, *111*, 15363–15369.

(21) (a) Disley, D. M.; Cullen, D. C.; You, H. X.; Lowe, C. R. *Biosens. Bioelectron.* **1998**, *13*, 1213–1225. (b) Mizutani, F.; Sato, Y.; Yabuki, S.; Sawaguchi, T.; Iijima, S. *Electrochim. Acta* **1999**, *44*, 3833–3838. (c) Mashazi, P. N.; Ozoemena, K. I.; Maree, D. A.; Nyokong, T. *Electrochim. Acta* **2006**, *51*, 3489–3494.

(22) (a) Dalmia, A.; Liu, C. C.; Savinell, R. F. *J. Electroanal. Chem.* **1997**, *430*, 205–214. (b) Wang, Y.; Luo, J.; Chen, H.; He, Q.; Gan, N.; Li, T. *Anal. Chim. Acta* **2008**, *625*, 180–187. (c) Chen, Y.; Guo, L.-R.; Chen, W.; Yang, X.-J.; Jin, B.; Zheng, L.-M.; Xia, X.-H. *Bioelectrochemistry* **2009**, *75*, 26–31. (d) Zheng, M.; Chen, Y.; Zhou, Y. M.; Tang, Y. W.; Lu, T. H. *Talanta* **2010**, *81*, 1076–1080.

(23) Scodeller, P.; Carballo, R.; Szamocki, R.; Levin, L.; Forchiassin, F.; Calvo, E. J. *J. Am. Chem. Soc.* **2010**, *132*, 11132–11140.

(24) Rouhana, L. L.; Jaber, J. A.; Schlenoff, J. B. *Langmuir* **2007**, *23*, 12799–12801.
(25) Kolega, R. R.; Schlenoff, J. B. *Langmuir* **1998**, *14*, 5469–5478.
(26) Persson, B. N. J. *Phys. Rev. B* **1991**, *44*, 3277–3296.
(27) (a) Worley, C. G.; Linton, R. W. *J. Vac. Sci. Technol., A* **1995**, *13*, 2281–2284. (b) Zhang, Y.; Terrill, R. H.; Tanzer, T. A.; Bohn, P. W. *J. Am. Chem. Soc.* **1998**, *120*, 2654–2655. (c) Norrod, K. L.; Rowlen, K. L. *J. Am. Chem. Soc.* **1998**, *120*, 2656–2657. (d) Zhang, Y.; Terrill, R. H.; Bohn, P. W. *Chem. Mater.* **1999**, *11*, 2191–2198. (e) Mirsaleh-Kohan, N.; Bass, A. D.; Sanche, L. *Langmuir* **2010**, *26*, 6508–6514.
(28) Hoogvliet, J. C.; Dijksma, M.; Kamp, B.; van Bennekom, W. P. *Anal. Chem.* **2000**, *72*, 2016–2021.
(29) (a) Weisshaar, D. E.; Lamp, B. D.; Porter, M. D. *J. Am. Chem. Soc.* **1992**, *114*, 5860–5862. (b) Shi, X.; Caldwell, W. B.; Chen, K.; Mirkin, C. A. *J. Am. Chem. Soc.* **1994**, *116*, 11598–9. (c) Calvente, J. J.; Kovacova, Z.; Sanchez, M. D.; Andreu, R.; Fawcett, W. R. *Langmuir* **1996**, *12*, 5696–5703. (d) Pesika, N. S.; Stebe, K. J.; Searson, P. C. *Langmuir* **2006**, *22*, 3474–3476.
(30) (a) Strong, L.; Whitesides, G. M. *Langmuir* **1988**, *4*, 546–558. (b) Chidsey, C. E. D.; Liu, G. Y.; Rowntree, P.; Scoles, G. *J. Chem. Phys.* **1989**, *91*, 4421–4423. (c) Chidsey, C. E. D.; Loiacono, D. N. *Langmuir* **1990**, *6*, 682–691. (d) Alves, C. A.; Smith, E. L.; Porter, M. D. *J. Am. Chem. Soc.* **1992**, *114*, 1222–1227.
(31) Bard, A. J.; Faulkner, L. R. *Electrochemical methods: Fundamentals and application*, 2nd ed.; John Wiley & Sons: New York, 2001.
(32) Schlenoff, J. B.; Dharia, J. R.; Xu, H.; Wen, L. Q.; Li, M. *Macromolecules* **1995**, *28*, 4290–4295.
(33) (a) Jung, L. S.; Campbell, C. T. *J. Phys. Chem. B* **2000**, *104*, 11168–11178. (b) Jung, L. S.; Campbell, C. T. *Phys. Rev. Lett.* **2000**, *84*, 5164–5167.
(34) (a) Vette, K. J.; Orent, T. W.; Hoffman, D. K.; Hansen, R. S. *J. Chem. Phys.* **1974**, *60*, 4854–4861. (b) Evans, S. D.; Urankar, E.; Ulman, A.; Ferris, N. *J. Am. Chem. Soc.* **1991**, *113*, 4121–4131. (c) Meakin, P.; Jullien, R. *Phys. A* **1992**, *187*, 475–488. (d) Evans, J. W. *Rev. Mod. Phys.* **1993**, *65*, 1281–1329.
(35) Somorjai, G. A. *Introduction to surface chemistry and catalysis*, 1st ed.; Wiley Inter-Science: New York, 1994.
(36) (a) Stranick, S. J.; Parikh, A. N.; Allara, D. L.; Weiss, P. S. *J. Phys. Chem.* **1994**, *98*, 11136–11142. (b) Mahaffy, R.; Bhatia, R.; Garrison, B. J. *J. Phys. Chem. B* **1997**, *101*, 771–773. (c) Imabayashi, S.; Hobara, D.; Kakiuchi, T. *Langmuir* **2001**, *17*, 2560–2563. (d) Biener, M. M.; Biener, J.; Friend, C. M. *Langmuir* **2005**, *21*, 1668–1671. (e) Cometto, F. P.; Paredes-Olivera, P.; Macagno, V. A.; Patrito, E. M. *J. Phys. Chem. B* **2005**, *109*, 21737–21748.
(37) (a) Herzog, G.; Arrigan, D. W. M. *Electroanalysis* **2003**, *15*, 1302–1306. (b) Herzog, G.; Arrigan, D. W. M. *Anal. Chem.* **2003**, *75*, 319–323.
(38) Russel, W. B.; Saville, D. A.; Schowalter, W. R. *Colloidal dispersions*, 1st ed.; Cambridge University Press: Cambridge, 1989.
(39) Calvente, J. J.; Lopez-Perez, G.; Jurado, J. M.; Andreu, R.; Molero, M.; Roldan, E. *Langmuir* **2010**, *26*, 2914–2923.
(40) Xu, S.; Laibinis, P. E.; Liu, G. Y. *J. Am. Chem. Soc.* **1998**, *120*, 9356–9361.
(41) Issa, Z. K.; Manke, C. W.; Jena, B. P.; Potoff, J. J. *J. Phys. Chem. B* **2010**, *114*, 13249–13254.